JACS
JOURNAL OF THE AMERICAN CHEMICAL SOCIETY

ARTICLE

pubs.acs.org/JACS

High Energy Ion Irradiation-Induced Ordered Macropores in Zeolite Crystals

Valentin Valtchev,*[,†] Emannuel Balanzat,[‡] Vesselina Mavrodinova,[#] Isabel Diaz,[⊥] Jaâfar El Fallah,[†] and Jean-Michel Goupil[†]

[†]Laboratoire Catalyse & Spectrochimie, UMR6506, ENSICAEN - Université de Caen - CNRS, 6 boulevard du Maréchal Juin, 14050 Caen, France

[‡]CIMAP Centre de recherche sur les Ions les Matériaux et la Photonique, UMR 6252 CEA/CNRS/ENSICAEN, BP 5133 14070 CAEN, France

[#]Institute of Organic Chemistry, Bulgarian Academy of Sciences, Acad. Bonchev str., Sofia 1113, Bulgaria

[⊥]Instituto de Catálisis y Petroleoquímica, CSIC, C/Marie Curie 2, Cantoblanco, 28049 Madrid, Spain

Supporting Information

ABSTRACT: The present study demonstrated the possibility to form a secondary system of parallel macropores in zeolite crystals. The secondary pore formation was predetermined by the creation of defect zones in ZSM-5 crystals. A high energy ^{238}U ion beam was employed to form latent tracks in zeolite crystals, which were further subjected to attack with diluted HF solution and thus developed to uniformally sized macropores. The selective extraction of material from latent tracks was due to the higher etching velocity of highly agitated zones created by heavy ion bombardment. The combination of complementary methods unambiguously demonstrated the formation of hierarchical zeolite material comprising parallel macropores that extended through the entire crystal. The catalytic tests revealed improved activity at retained selectivity in the reaction of *m*-xylene conversion. The possibility to control the number of macropores per unit of crystal surface and thus the catalytic performance of the material was demonstrated. This model material is expected to bring better understanding to the effect of a secondary pore system in the catalytic performance of hierarchical zeolites obtained by the top-down or bottom-up approach.

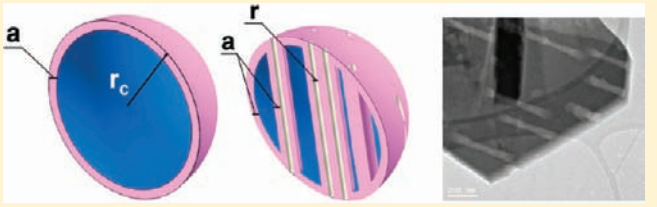

INTRODUCTION

The extraordinary selectivity of zeolite-based catalysts is often coupled with undesirable effects such as diffusion limitation, pore blocking, and catalyst deactivation. Two major avenues are considered to circumvent these drawbacks and fully explore the potential of zeolitic materials. The expectations for better performance are namely related to the use of nanocrystals and the preparation of conventional micrometer-sized zeolite crystals comprising larger (meso or macro) pores. Hydrothermal stability of zeolite nanocrystals is not always comparable with that of their micrometer-sized counterparts. In addition, zeolite nanoparticles are still not readily available. Consequently, in recent years, a lot of research has been dedicated to the controlled formation of a secondary pore network in different types of zeolite crystals. Different synthetic routes employed in the preparation of hierarchical zeolites can be classified into two groups, a top-down and a bottom-up approach.

The top-down approach is based on the preferential extraction of a framework cation and thus the formation of defects of meso- and/or macropore dimensions of zeolite crystals. In other words, the zeolite framework is subjected to demetalation, and the choice of the cation subjected to chemical attack depends on the composition of the zeolite. Low silica zeolites are usually subjected to dealumination by vapor steaming and/or acid treatment.[1−7] Lately, more works have been devoted to the desilication of high silica zeolites in basic media.[8−14]

The bottom-up approach is a part of the template strategy, where sacrificial species are integrated in the growing crystals and then eliminated in a second step, leaving behind an empty space that represents a negative replica of the template. The template approach, first employed for the preparation of zeolite-type materials, where small organic molecules are used for directing the microporosity,[15] was extended to the formation of mesoporous[16] and macroporous[17] structures. By employing dual templates, hierarchical materials with combinations of micro-meso,[18] meso-macro,[19] micro-macro,[20] and micro-meso-macro[21] pores were synthesized. Carbon particles of different size and morphology have been the most widely used templates for the preparation of mesoporous zeolite crystals.[22] The employment of carbon nanotubes or fibers as sacrificial templates led to the formation of uniformly sized pores that correspond to the diameter of the templating filament.[23] However, their distribution within an

Received: August 29, 2011
Published: October 13, 2011

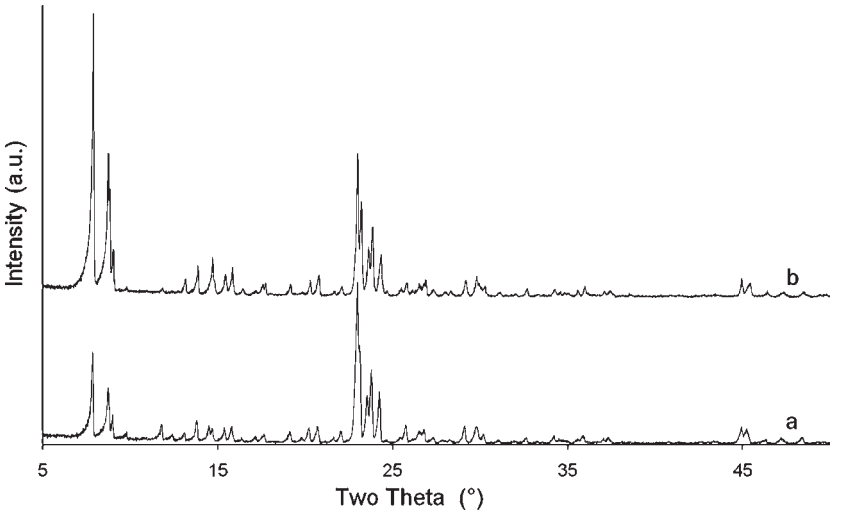

Figure 1. XRD patterns of the initial ZSM-5 sample (a) and the hierarchical material obtained by ^{238}U irradiation, HF etching, and calcination at 550 °C (b).

individual crystal and in the bulk product could not be controlled. Very recently, Ryoo and co-workers[24] and Okubo and co-workers[25] have provided examples of the application of supramolecular templates in the preparation of zeolites with hierarchical porosity. Recently, Tsapatsis and co-workers employed a new bottom-up approach to synthesize zeolite nanocrystals with three-dimensional ordered mesopores.[26] Microporous crystals with ordered mesopores were prepared by a multistep procedure where silica nanobeads were first employed to grow a colloidal crystal, and then a carbon replica of colloidal crystal was obtained and used as a sacrificial template to synthesize three-dimensionally ordered mesoporous-imprinted zeolite crystals.

Each of the above approaches offers certain advantages and disadvantages. None of them, however, could provide straight parallel macropores of similar size that extend through the zeolite crystals. The preparation of such a hierarchical material is indispensable to clearly evaluate the impact of the secondary pore network on the catalytic performance of zeolite catalysts. The present work involves the preparation of hierarchical zeolites with uniform size macropores by a top−down approach. The preparation of the uniform macropores is based on defect formation in zeolite crystals by bombardment with swift heavy ions. In most dielectric solids, the impact of swift heavy ions (SHI), with typical energies above hundreds of MeV and masses around or above 100, induces an irreversible material transformation along each projectile path. This damaged region, referred to as "latent track" or "nuclear track", has a cylindrical shape, with diameters ranging from a few nanometers to a few tens of nanometers and is created all along the major part of the ion range. Depending on their energy and mass, SHI have ranges from some tens to some hundreds of micrometers. Etching in a suitable chemical agent opens a micro- or nanohole all along the ion path "etched tracks".[27a] Industrial production of polymer membranes (track-etched membranes) that started in the early 1970s is still very active nowadays.[27b,c] New uses emerged more recently. For instance, track-etched films are used as templates for engineered nanoobjects for use in microwave and electronic devices and biomedical sensing.[27d,e] Latent or etched tracks can also be grafted and used in fuel cells.[27f] However, to the best of our knowledge, the ion track technology has never been applied for inducing a secondary pore network in zeolite crystals and to obtain hierarchical porous catalysts. Owing to high chemical uniformity of micrometer-sized zeolite crystals, a uniform dissolution and thus the formation of similar in size pores can be expected. The length of the track depends on the employed ion and the target material. In the case of silicates, it exceeds hundreds of micrometers, which is sufficient to create extended defects throughout the entire crystal. The pore diameter may range from about 10 nm to 1 μm or more depending on the employed swift heavy ion and the etching conditions. In general, the resultant channels are parallel to within several degrees. Areal density can range between 1 and more than 1010 channels per cm^2. Usually the channels are statistically distributed over the irradiated area of the sample. The present report describes a two-step top-down approach, involving formation of latent tracks and their selective extraction by wet chemical treatment that provides parallel uniform macropores in zeolite crystals.

EXPERIMENTAL SECTION

ZSM-5 crystals were prepared in fluoride media from a gel with composition $0.2(C_3H_7)_4NBr{:}0.07Al_2O_3{:}1.0SiO_2{:}0.58NH_4F{:}15H_2O$, where $(C_3H_7)_4NBr$ is tetrapropylammonium bromide (Fluka). The other reactants were provided by Merck (93.5 wt % SiO_2), Reheis (AlOOH, pseudoboehmite), and Fluka (NH_4F). After the initial reactants were mixed, 2 wt %, with respect to silica content in the gel, of nanosized silicalite-1 seeds was added to the mixture and stirred 1 h. The synthesis was performed at 170 °C for 10 days. After washing and drying, the product was subjected to ^{238}U irradiation under vacuum. Latent tracks are induced in most insulators where the linear energy transfer (LET) is above a threshold value. The ion and energy were chosen to ensure irradiation of a sufficient amount of matter with a large LET. The entrance and exit energies of the ions are 4.75 and 1.25 GeV, respectively. The mean LET is 30 keV/nm, and the LET variation along the sample is approximately less than 20%. Latent track development was performed with 0.1 wt % HF acid at room temperature for 5 min. The liquid:solid ratio was 50:1. The solid was thoroughly washed with distilled water and dried at 60 °C.

As-synthesized and treated materials were characterized by X-ray diffraction (X'Pert Pro, PANalytical) scanning (TESCAN) and transmission (JEOL JEM 2100F) electron microscopy and N_2 adsorption (Micromeritics ASAP 2020). The chemical composition of the solids was analyzed by atomic absorption spectroscopy (AAS) (Varian Techtron AA6).

The catalytic tests were carried out in a fixed-bed flow reactor at atmospheric pressure and reaction temperature of 623 K. N_2 carrier gas was passed through a saturator filled with *m*-xylene and equilibrated at 293.2 K so a reactant partial pressure of 0.9 kPa could be attained. Online analysis of the reaction products has been performed using HP-GC with a 25 m FFAP capillary column.

RESULTS AND DISCUSSION

The new preparation method reported here is based on the preferential etchability of latent tracks. More precisely the preparation of macropores in zeolite crystals includes two stages: (i) exposing zeolite crystals to a flow of swift heavy ions for inducing latent tracks; (ii) etching the latent tracks to create meso- or macropores. An important feature of the technique is that one single particle is sufficient to create a damaged zone in the zeolite crystal, which is characterized with high free energy. Substantially different etching velocity of the latent ion track and the intact part of the crystals allows selective extraction of the amorphous part of the crystal and thus controlled pore formation. Therefore, the physical treatment tracks down the pore formation during the following wet chemical treatment. The method is exemplified by the formation of parallel macropores in ZSM-5 crystals. The formation of meso-/macropores of heavily intergrown aggregates is difficult to study. Therefore, well-shaped single crystals grown in fluoride media were employed to clearly visualize the mesopores issued from the nuclear track imprinting. The size of the crystals was about 5 μm along the *c* axis. Zeolite crystals were exposed to ^{238}U ion beam with fluencies corresponding to an average distance between ion impacts of 230, 700, and 1400 nm. The irradiated samples were then etched with diluted HF acid and thoroughly washed with distilled water. Note that after the irradiation, the residual radioactivity is below the civil norms and the material can be used without any particular safety precautions.

XRD study of irradiated samples did not show any differences with that of the parent ZSM-5 crystals (Figure 1a). The irradiated material was subjected to HF etching and calcination at 550 °C. The XRD pattern of the resultant hierarchical material is shown in Figure 1b. As can be seen by the XRD pattern, the crystallinity of the sample was retained and no amorphous halo was observed.

Scanning electron microscopy (SEM) analysis of irradiated and etched samples showed the presence of large pores with uniform pore openings on the surface of the crystals (Figure 2a,b). According to the SEM inspection, the pore size was about 50 nm. For the sake of comparison, nonirradiated crystals were subjected to the same treatment and studied by SEM. Low and high magnification images of ZSM-5 crystals subjected to this treatment are shown in Figure 2c,d. The SEM analysis clearly revealed that without preliminary treatment, only surface etching occurred while in the case of irradiated samples, highly uniform sized pores were formed. A closer look at the hierarchical sample showed that the distance between ion impacts was uniform in some crystals and less uniform in others, the latter being a consequence of the low ion beam stability during the experiment. Thus, much more uniform distribution of macropores is expected under standard irradiation conditions.

Transmission electron microscopy (TEM) investigations confirmed that the diameter of the pores was about 50 nm (Figure 3a−d), a value at the border between meso- and macroporous materials. TEM observations also revealed that the pore diameter was constant along the crystal length

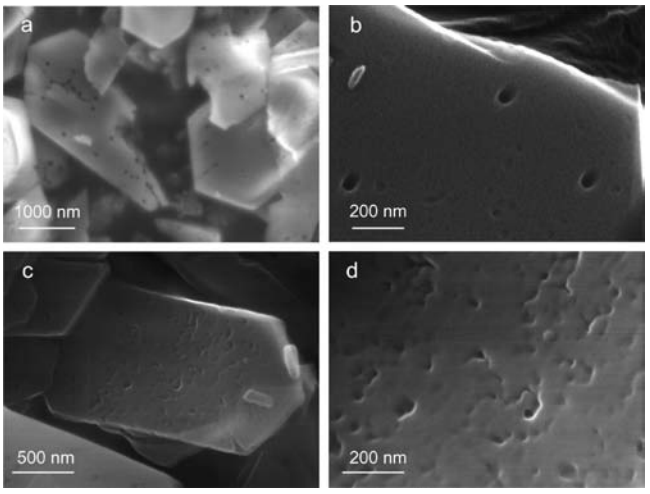

Figure 2. Low (a) and high (b) magnification SEM micrographs of ZSM-5 crystals subjected to irradiation and acid etching. Low (c) and high (d) magnification micrographs of a ZSM-5 crystal subjected to similar acid treatment without preliminary ion beam irradiation.

(Figure 3a,c). The formation of parallel pores of similar size that cross the entire zeolite crystal was sound proof for the decisive effect of the ion beam treatment on the following chemical extraction step. The latter was proved by an experiment where nonirradiated ZSM-5 crystals were subjected to similar chemical attacks. Exclusively, the surface of the nonirradiated crystals was etched (Figure 3e,f) as already shown by the SEM investigation. A deeper dissolution was observed only in a zone which most probably comprised a high concentration of framework defects (Figure 3e). Shaped crystals employed in the present study possessed well-developed 010 and 100 faces. Consequently, most of the irradiated crystals possessed latent tracks parallel to one of well-developed crystal faces (Figure 3a,b). Thus, the differences in the secondary pore network orientation were a consequence of the orientation of the crystals during the irradiation step. Prior to the ^{238}U beam treatment, the zeolite powder was pressed in a holder, and thus the crystals were oriented with the well-developed crystal faces perpendicular to the applied force. Hence, the preferential orientation of pressed zeolite crystals could be used to trace the secondary pore system in the desired crystallographic direction. There are also more sophisticated surface functionalization methods that allow the formation of layers of oriented zeolite crystals and thus control the pore orientation.[28] High resolution TEM inspection of macropores revealed another important feature of ion beam-induced pores. There is division between the large pore channel and the intact part of the zeolite framework (Figure 3g,h). In other words, there is not a transition zone comprising a highly defected or partially amorphisized framework because of the preferential extraction of some of the framework components or the high temperature combustion of a carbon-rich sacrificial template.

Uniform extraction of framework components was confirmed by the chemical analyses of initial (Si/Al = 26.9) and hierarchical (Si/Al = 28.0) zeolites. Note that post synthesis chemical etching (desilication or dealumination) leads to preferential extraction of one of framework cations that may dramatically change the activity of zeolite catalysts. In the present case, the formation of defect zones prior to chemical treatment makes possible the uniform extraction of framework cations. Another important

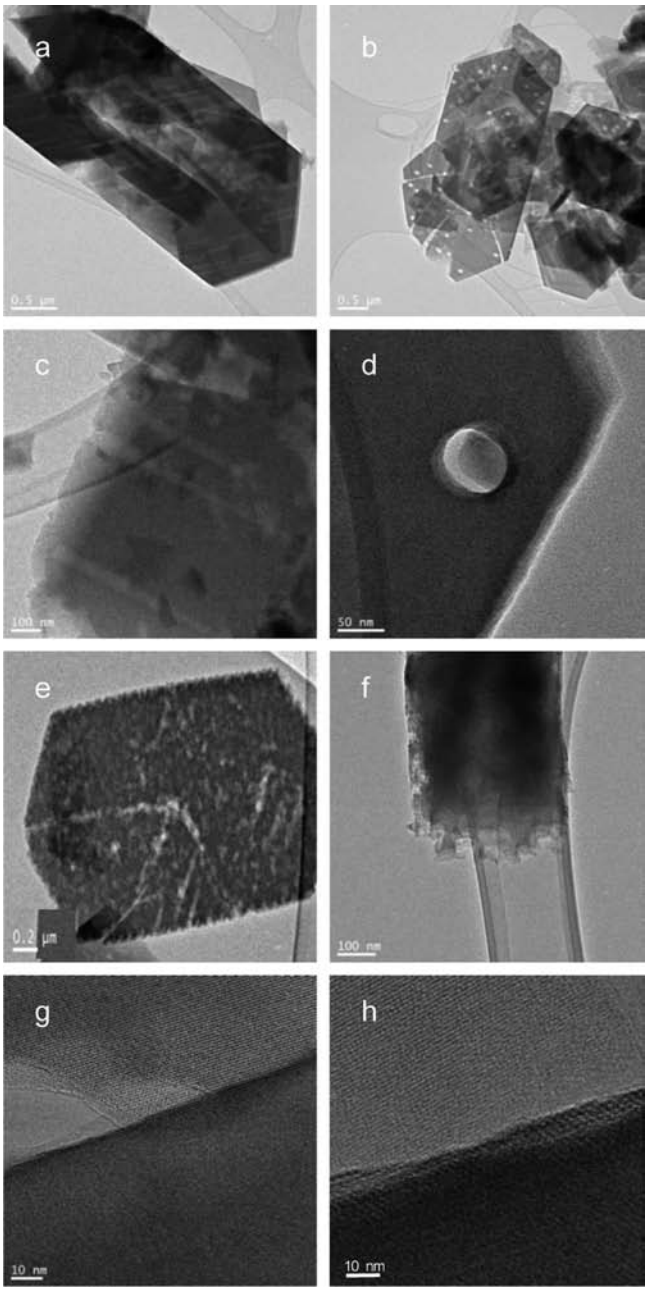

Figure 3. TEM micrographs of ZSM-5 crystals with ordered systems of macropores (a and b) obtained by ^{238}U irradiation followed by diluted HF acid etching. Side (c) and top (d) views of the macropores in ZSM-5 crystals showing that the pore diameter is around 50 nm. Low (e) and high (f) magnification TEM micrographs of nonirradiated ZSM-5 crystals subjected to treatment with diluted HF acid. High resolution TEM images of the secondary channel system where the border between the macropore and the intact part of the crystal can be seen (g and h).

feature of the method is that the extraction of the amorphous material is not influenced by the defect and intergrown surfaces in the crystal. Figure 3a shows that the macropore channels traversing the 90° twin crystal remained parallel to the ion track orientation.

The N_2 adsorption measurements were in good agreement with the TEM investigation. Figure 4 shows the N_2 adsorption isotherms of parent ZSM-5 crystals and hierarchical material with

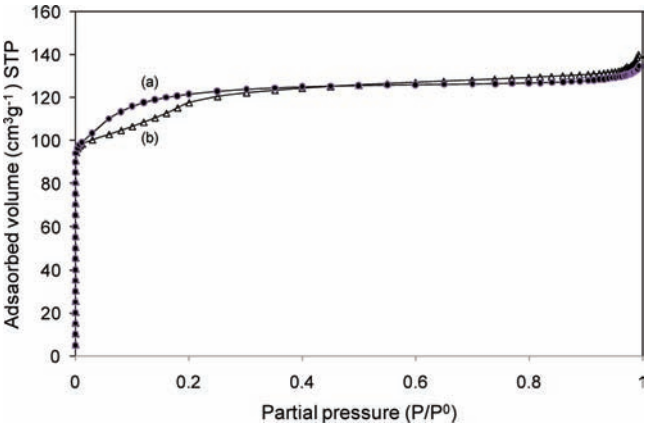

Figure 4. N_2 adsorption−desorption isotherms of the parent ZSM-5 crystals (a) and the hierarchical zeolite material comprising the secondary system of macropores with an average distance of 230 nm between them (b).

an average distance of 230 nm between the large pore channels. Type I adsorption−desorption isotherms, typical of microporous zeolite-type materials, were recorded for both materials. A steep rise in the uptake at low relative pressures corresponds to the filling of micropores with N_2. This part of the isotherm was followed by a transition zone between 0.05 and 0.25 P/P^0, where a substantial difference between the two isotherms was observed. In the case of MFI-type materials, this part of the curve corresponds to adsorbate transition from a more disordered fluid-like to a more ordered solid-like phase.[29] Obviously the kinetics of this phenomenon is different in the presence of large pores crossing the volume of zeolite crystals, which explains the differences observed in this part of the isotherm. In the 0.3−1.0 P/P^0 range, the two isotherms are almost flat without a hysteresis loop. A negligible uptake can be observed at a relative pressure close to 1, which is more pronounced in the case of hierarchical zeolites. This last upward turn of the isotherm indicates the presence of very large pores. Both materials possessed micropore volumes of 0.18 $cm^3\ g^{-1}$ that are characteristic of highly crystalline MFI-type material. This result clearly showed that the formation of a secondary pore network was not at the expense of the micropore volume of the material. In other words, the formation of a few macropores per single crystal did not substantially change either the micropore volume or the external surface area of the solid. Indeed, the analysis of the N_2 adsorption data revealed a negligible increase in the external surface area of the hierarchical zeolite sample (from 0.4 $m^2\ g^{-1}$ to 8 $m^2\ g^{-1}$). Low mesopore volume (0.03 $cm^3\ g^{-1}$) was also indirect proof of the formation of very large pores in zeolite crystals. As mentioned previously, the pore diameter was about 50 nm (Figure 3c,d), which made N_2 adsorption measurements inapplicable to this pore size regime. Formation of narrower (meso)pores will certainly be possible by varying the etching solution concentration and time−temperature conditions of the treatment, which is not in the scope of the present study.

The materials subjected to irradiation at different fluencies, in other words with a different number of ion tracks per unit surface, were subjected to chemical treatment under similar conditions. After calcination, the resultant materials with an average distance between pores of 230, 700, and 1400 nm were subjected to catalytic tests in the reaction of *m*-xylene conversion (Figure 5).

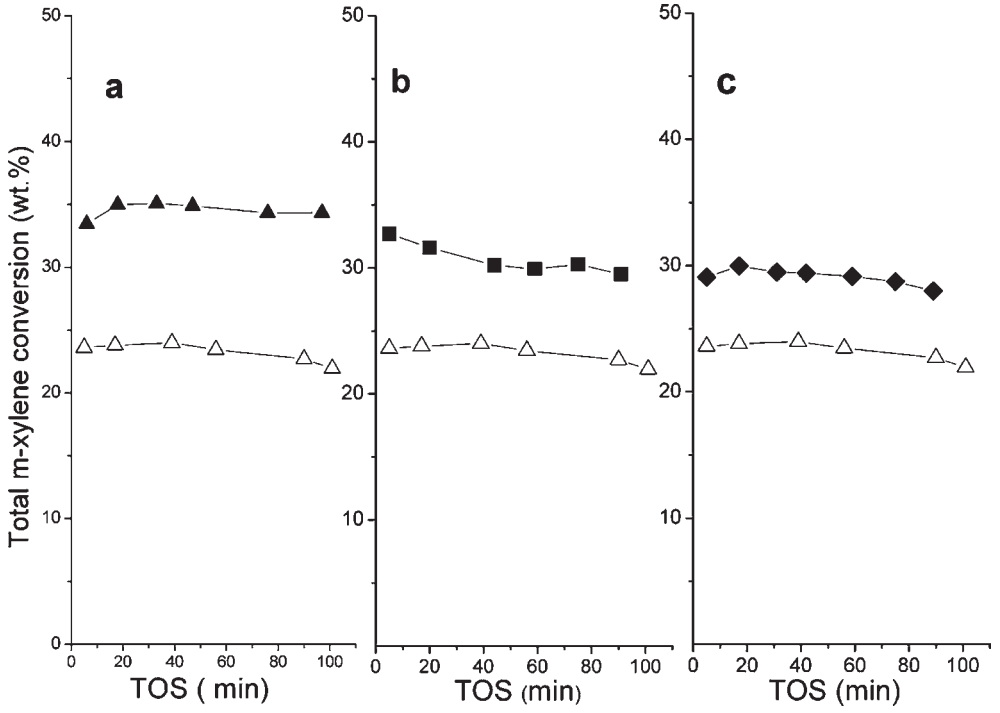

Figure 5. Total *m*-xylene conversion as a function of the time on-stream over the initial ZSM-5 sample (empty triangles) and the mesoporous zeolites with an average distance between the secondary pore systems of 230 nm (a), 700 nm (b), and 1400 nm (c). (Reaction temperature 623 K, contact time 0.82 h).

The material with an average macropore distance of 230 nm showed a higher *m*-xylene conversion with respect to the initial nontreated ZSM-5 catalysts and the two materials with less mesopores per unit zeolite surface. Obviously, the procedure applied to develop denser intracrystalline macroporosity has had a more beneficial effect on the catalytic performance.

Thus, the facilitated access of the reactant and its improved transport, together with that of the reaction products through a denser system of macropores, appeared to be the dominating factor for the observed improvement in the catalytic behavior of the hierarchical zeolite materials prepared by the new method. These results were also in accordance with the findings of Christensen and co-workers,[30] who have studied mesostructured materials obtained by using a mesoporous carbon matrix in the same reaction of *m*-xylene conversion.

A simple model has been developed for estimating the gain in activity that could be expected by etched latent tracks when the activity of the substrate was limited by the diffusion of the reactant over a layer of thickness "a". The principle of the model is demonstrated in Figure 6, and the final formulas employed in calculating the gain in activity are provided in Supporting Information. The specific activity is the ratio between the pink and blue volumes, and the gain is the ratio between the so-defined specific activities, after and before track etching. The experimental data in total *m*-xylene conversion obtained with hierarchical ZSM-5 materials comprising different number of macropores per unit crystal surface fitted well to the model (Figure 1, Supporting Information). Thus theoretical and experimental data pointed out the positive effect of macropore network on the catalytic performance of a zeolitic catalyst.

To evaluate the effect of the modification procedure, the catalysts' performance at a close degree of conversion (Figure 7a)

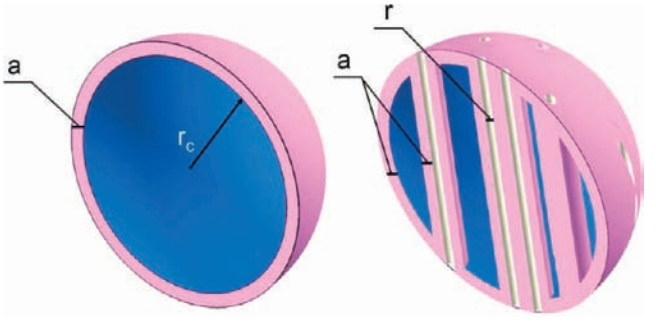

Figure 6. Part of the zeolite crystal available for catalytic reaction: before (left) and after (right) latent track etching.

was put together. In the range of tested reaction temperatures and contact times, only traces of side products (under the detection limit) were observed. The main products expected from *m*-xylene isomerization (para and ortho isomer) and disproportionation (toluene and trimethylbenzenes) constituted over 99.99% of the reaction product. In accordance with the product shape-selectivity effect of the MFI-type zeolites, only the slimmest and most thermodynamically preferred from the three trimethylbenzenes isomers, the 1,2,4-one, was formed on both studied catalysts. The distinguishing characteristics such as the *p*- to *o*-xylene ratio and the selectivity to the main isomerization and the side disproportionation reactions of *m*-xylene transformation were also compared (Figures 7b,c). As typical of ZSM-5, a bit higher than the equilibrium *p*-/*o*-xylene ratio (Figure 7b) and a much larger selectivity to isomerization compared to disproportionation (Figure 7c) were observed both on the parent and the modified catalysts.

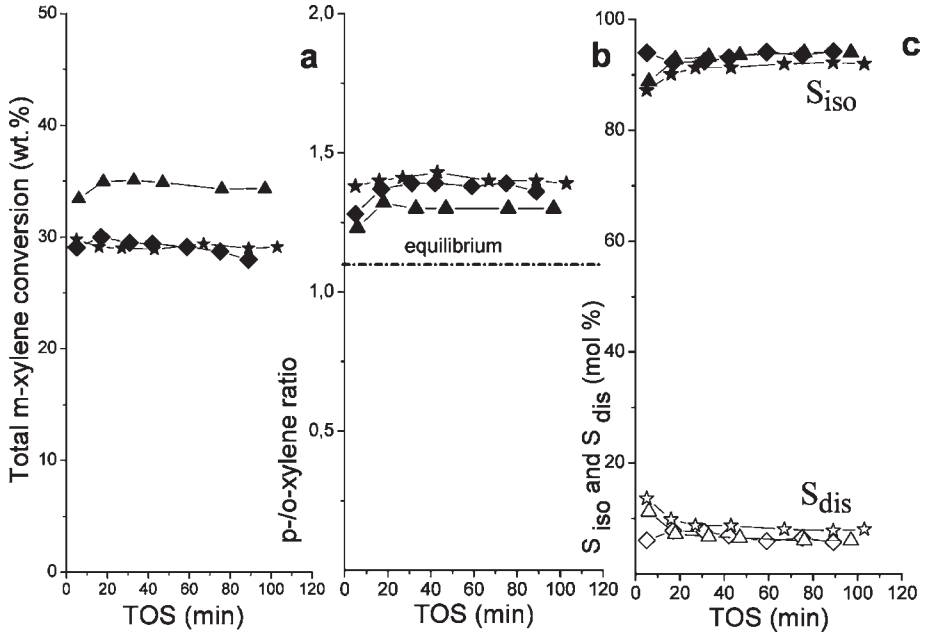

Figure 7. Total *m*-xylene conversion (a), *p*-/*o*-xylene ratio (b), and selectivity to isomerization (S_{iso}) and disproportioination (S_{dis}) (c), as a function of the time on-stream over the parent (star) and the macroporous zeolites with an average distance between the secondary pore systems of 230 nm (triangle) and 1400 nm (rhombus). (Reaction temperature 623 K, contact time 0.82 h for the modified catalysts, and 1.3 h for the parent material).

The very close values of these characteristics proved the uniform extraction of framework compounds upon development of a secondary pore system as mentioned above. This result was also in accordance with the similar external surface area and pore volume registered for the initial and hierarchical ZSM-5 samples. Indeed, N_2 adsorption measurements showed that the formation of macropores was not at the expense of the micropore volume and the surface area was not changed substantially, both structure characteristics determining the selectivity in the reactions of *m*-xylene transformation.[31] Thus, the macropores serve as additional diffusion pathways only, facilitating the mass transfer and thus improving the catalytic activity of the hierarchical materials. This result is in agreement with the activity gain model, which showed that the external surface area of a hierarchical zeolite material strongly depends on the size of the pores (Figure 2, Supporting Information). Namely, a large number of small size mesopores substantially increases the external surface area of zeolite crystals that often have a negative effect on the isomerization selectivity and respectively on the *p*-xylene formation in the reaction of *m*-xylene conversion. Therefore, the formation of a few macropores traversing the entire zeolite crystal could provide access to substantial part of micropore volume without increasing the external surface area. This is an important result that should be taken into account when the goal is the preparation of zeolite catalysts combining high selectivity with high catalytic activity.

CONCLUSIONS

In conclusion, the present study proved the possibility to form uniform parallel macropores in zeolite crystals. The secondary pore system formation was predetermined by creation of defect zones in the crystals vulnerable to chemical attack. A high energy ^{238}U ion beam was employed to form latent tracks in the crystals, which were further subjected to attack with diluted HF solution to extract the amorphous material and form regular size macropores.

The catalytic tests showed the versatility of the method, allowing the number of macropores per unit crystal surface to be controlled and thus the catalytic activity of such preparations to be finely tuned. These materials are also expected to show better performance with respect to solely microporous materials in a variety of areas, from traditional ion exchange, sorption, and catalytic processes to much more advanced applications ranging from chemical sensing to drug delivery. Ion beam-induced meso- or macropores could also be applied to intergrown zeolite films largely used in membrane and sensing devices. The amorphization of a part of the zeolite framework by ion bombardment might also be employed to prepare functional materials comprising zones with different structure and/or composition within a single zeolite crystal.

ASSOCIATED CONTENT

Supporting Information. Formulas employed in the activity gain model, and graphs presenting the gain in activity as a function of the fluence and the size of secondary pores. This material is available free of charge via the Internet at http://pubs.acs.org.

AUTHOR INFORMATION

Corresponding Author
valtchev@ensicaen.fr

ACKNOWLEDGMENT

The project was partially sponsored by the French Research Agency (ANR) project HiZeCOKE (contract ANR-2010-BLAN-723). V.V. and I.D. acknowledge French−Spanish bilateral program PICASSO (No. 19216QK and HF2008-0066).

REFERENCES

(1) Lynch, J.; Raatz, F.; Dufresne, P. *Zeolites* **1987**, *7*, 333.
(2) Patzelova, V.; Jeager, N. I. *Zeolites* **1987**, *7*, 240.
(3) Lynch, J.; Raatz, F.; Delalande, Ch. *Stud. Surf. Sci. Catal.* **1988**, *39*, 547.
(4) Maher, P. K.; Hunter, F. D.; Scherzer, J. *Adv. Chem. Ser.* **1971**, *101*, 266.
(5) Cartlidge, S.; Nissen, H. U.; Wessicken, R. *Zeolites* **1989**, *9*, 346.
(6) Sasaki, Y.; Suzuki, T.; Takamura, Y.; Saji, A.; Saka, H. *J. Catal.* **1998**, *178*, 94.
(7) Choi-Feng, C.; Hall, J. B.; Higgins, B. J.; Begerlein, R. A. *J. Catal.* **1993**, *140*, 395.
(8) Dessau, R. M.; Valyocsik, E. W.; Goeke, N. H. *Zeolites* **1992**, *12*, 776.
(9) Cizmic, A.; Subotic, B.; Smit, I.; Toneic, A.; Rosario, A.; Crea, F.; Nastro, A. *Microporous Mater.* **1997**, *8*, 159.
(10) Ogura, M.; Shinomiya, S. Y.; Tateno, J.; Nara, Y.; Kikuchi, E.; Matsukata, H. *Chem. Lett.* **2000**, 82.
(11) Lietz, G.; Schnabel, K. H.; Peuker, C.; Gross, T.; Storek, W.; Völter, J. *J. Catal.* **1994**, *148*, 562.
(12) Chang, C. D.; Chu, C. T. W. US Patent 4594333, 1986.
(13) Graces, J. M.; Millar, D. M. US Patent 60175908, 1998.
(14) (a) Groen, J. C.; Jansen, J. C.; Moulijn, J. A.; Perez-Ramirez, J. *J. Phys. Chem. B* **2004**, *108*, 13062. (b) Groen, J. C.; Peffer, L. A. A.; Moulijn, J. A.; Perez-Ramirez, J. *Colloids Surf., A* **2004**, *241*, 53. (c) Groen, J. C.; Peffer, L. A. A.; Moulijn, J. A.; Perez-Ramirez, J. *Chem.—Eur. J.* **2005**, *11*, 4983. (d) Groen, J. C.; Bach, T.; Zeise, U.; van Donc, A.M. P.; de Jong, K. P.; Moulijn, J. A.; Perez-Ramirez, J. *J. Am. Chem. Soc.* **2005**, *127*, 10792. (e) Groen, J. C.; Maldonado, L.; Berrier, E.; Brückner, A.; Moulijn, J. A.; Perez-Ramirez, J. *J. Phys. Chem. B* **2006**, *110*, 20369. (f) Groen, J. C.; Zhu, W.; Brouwer, S.; Huynink, S. J.; Kapteijn, F.; Moulijn, J. A.; Perez-Ramirez, J. *J. Am. Chem. Soc.* **2007**, *129*, 355. (g) Groen, J. C.; Sano, T.; Moulijn, J. A.; Perez-Ramirez, J. *J. Catal.* **2007**, *251*, 21. (h) Groen, J. C.; Abello, S.; Villaescusa, L.; Perez-Ramirez, J. *Microporous Mesopororous Mater.* **2008**, *114*, 93.
(15) Szostak, R. in *Molecular Sieves*, 2nd ed.; Blackie Academic & Professional: London, 1998; p 359.
(16) Vartuli, J. C.; Roth, W. J.; Beck, J. S.; McCullen, S. B.; Kresge, C. T. In *Molecular Sieves: Science and Technology*; Karge, H. G.; Weitcamp, J., Eds.; Springer: Berlin, 1998; Vol. I, p 97.
(17) Velev, O. D.; Kaler, E. W. *Adv. Mater.* **2000**, *12*, 531.
(18) Tosheva, L.; Valtchev, V.; Sterte, J. *Microporoous Mesopo-rorous Mater.* **2000**, *35*−*36*, 621.
(19) Velev, O. D.; Tessier, P. M.; Lenhoff, A. M.; Kaler, E. W. *Nature* **1999**, *401*, 548.
(20) Lee, Y.-J.; Lee, J. S.; Park, Y. S.; Yoon, K. B. *Adv. Mater.* **2001**, *13*, 1259.
(21) Rhodes, K. H.; Davis, S. A.; Caruso, F.; Zhang, B.; Mann, S. *Chem. Mater.* **2000**, *12*, 2832.
(22) (a) Jacobsen, C. J. H.; Madsen, C.; Houzvicka, J.; Schmidt, I.; Carlsson, A. *J. Am. Chem. Soc.* **2000**, *122*, 7116. (b) Janssen, A. H.; Schmidt, I.; Jacobsen, C. J. H.; Koster, A. J.; de Jong, K. P. *Microporous Mesoporous Mater.* **2003**, *65*, 59. (c) Boisen, A.; Schmidt, I.; Carlsson, A.; Dahl, S.; Brorson, M.; Jacobsen, C. J. H. *Chem. Commun.* **2003**, 958. (d) Christensen, C. H.; Johannsen, K.; Törnkvist, E.; Schimdt, I.; Topsoe, H.; Christensen, C. H. *Catal. Today* **2007**, *128*, 117. (e) Christensen, C. H.; Johannsen, K.; Schimdt, I.; Christensen, C. H. *J. Am. Chem. Soc.* **2003**, *125*, 13370.
(23) (a) Schmidt, I.; Boisen, A; Gustavsson, E.; Stahl, K.; Pehrson, S.; Dahl, S.; Carlsson, A.; Jacobsen, C. J. H. *Chem. Mater.* **2001**, *13*, 4416. (b) Boisen, A.; Schmidt, I.; Carlsson, A.; Dahl, S.; Brorson, M.; Jacobsen, C. J. H. *Chem. Commun.* **2003**, 958. (c) Janssen, A. H.; Schimdt, I.; Jacobsen, C. J. H.; Koster, A. J.; de Jong, K. P. *Microporous Mesoporous Mater.* **2003**, *65*, 59.
(24) (a) Choi, M.; Cho, H. S.; Srivastava, R.; Venkatesan, C.; Choi, D. H.; Ryoo, R. *Nature Mat.* **2006**, *5*, 718. (b) Cho, K.; Cho, H. S.; de Ménorval, L.-C.; Ryoo, R. *Chem. Mater.* **2009**, *21*, 5664.
(25) Mukti, R. R.; Hirahara, H.; Sugawara, A.; Shimojima, A.; Okubo, T. *Langmuir* **2010**, *26*, 2731.
(26) (a) Fan, W.; Snyder, M. A.; Kumar, S.; Lee, P.-S.; Yoo, W. C.; McCormick, A. V.; Penn, R. L.; Stein, A.; Tsapatsis, M. *Nat. Mater.* **2008**, *7*, 984. (b) Chen, H.; Wydra, J.; Zhang, X.; Lee, P.-S; Wang, Z.; Fan, W.; Tsapatsis, M. *J. Am. Chem. Soc.* **2011**, *133*, 12390. (c) Liu, D.; Bhan, A.; Tsapatsis, M.; Al Hashimi, S. *Catalysis* **2011**, *1*, 7.
(27) (a) Fischer, B. E.; Spohr, R. *Rev. Mod. Phys.* **1983**, *55*, 907. (b) Fleisher, R. L. *Tracks to Innovation; Nuclear Tracks in Science and Technology*; Springer: New York, 1998. (c) Hano, H.; Ferain, E. *Nucl. Instr. Methods Phys. Res., Sect. B* **2009**, *267*, 1019. (d) Ferain, E.; Legras, R. *Nucl. Instr. Methods Phys. Res., Sect. B* **2009**, *267*, 1028. (e) Toulemonde, M.; Trautmann, C.; Balanzat, E.; Hjort, K; Weidinger, A. *Nucl. Instr. Methods Phys. Res., Sect. B* **2004**, *216*, 1. (f) Clochard, M.; Berthelot, C. T.; Baudin, C.; Betz, N.; Balanzat, E.; Gébel, G.; Morin, A. *J. Power Sources* **2010**, *195*, 223.
(28) Lee, J. S.; Lee, Y.-J.; Tae, E. L.; Park, Y. S.; Yoon, K. B. *Science* **2003**, *301*, 818.
(29) (a) Nakai, K.; Sonoda, J.; Yoshida, M.; Hakuman, M.; Naono, H. *Adsorption* **2007**, *13*, 351. (b) Llewellyn, P. L.; Coulomb, J.-P.; Grillet, Y.; Patarin, J.; Andre, G.; Rouquerol, J. *Langmuir* **1993**, *9*, 1852. (c) Voogd, P.; Scholten, J. J. F.; van Bekkum, H. *Colloids Surf.* **1991**, *55*, 163.
(30) Schmidt, I.; Christensen, C. H.; Hasselriis, P.; Kustova, M. Yu.; Brorson, M.; Dahl, S.; Johannsen, K.; Christensen, C. *Stud. Surf. Sci. Catal.* **2005**, *158*, 1247.
(31) (a) Jacobs, P.; Martens, J. *Proceedings of the 7th International Zeolites Conference*, Tokyo, Japan, 1986, p 23. (b) Corma, A.; Corell, C.; Martinez, A.; Perez-Pariente, J. In *Zeolites and related microporous materials: state of the art 1994*; Weitkamp, J.; Karge, H.G.; Pfeifer, H.; Holderich, W., Eds. *Stud. Surf. Sci. Catal.* **1994**, *84*, 859.